Heterogeneity and excitability of *BRAF^V600E*-induced tumors is determined by Akt/mTOR-signaling state and *Trp53*-loss

Silvia Cases-Cunillera, Karen M. J. van Loo, Julika Pitsch, Anne Quatraccioni, Sugirthan Sivalingam, Paolo Salomoni, Valeri Borger, Dirk Dietrich®, Susanne Schoch, and Albert J. Becker

Institute of Neuropathology, Section for Translational Epilepsy Research, Medical Faculty, University of Bonn, Bonn, Germany (S.C.-C., K.M.J.v.L., A.Q., S.Schoch, A.J.B.); Department of Epileptology, Neurology, RWTH Aachen University, Aachen, Germany (K.M.J.v.L.); Department of Human Genetics, Medical Faculty, University of Bonn, Bonn, Germany (S.Sivalingam); Nuclear Function Group, German Centre for Neurodegenerative Diseases (DZNE), Bonn, Germany (P.S.); Department of Neurosurgery, University Hospital Bonn, Bonn, Germany (V.B., D.D.); Department of Epileptology, Medical Faculty, University of Bonn, Bonn, Germany (J.P., S.Schoch)

Corresponding Author: Albert J. Becker, MD, Institute of Neuropathology, Section for Translational Epilepsy Research, Medical Faculty, University of Bonn, Venusberg-Campus 1, D-53127 Bonn, Germany (albert_becker@uni-bonn.de).

Abstract

Background. Developmental brain tumors harboring *BRAF^V600E* somatic mutation are diverse. Here, we describe molecular factors that determine *BRAF^V600E*-induced tumor biology and function.

Methods. Intraventricular in utero electroporation in combination with the piggyBac transposon system was utilized to generate developmental brain neoplasms, which were comprehensively analyzed with regard to growth using near-infrared in-vivo imaging, transcript signatures by RNA sequencing, and neuronal activity by multielectrode arrays.

Results. *BRAF^V600E* expression in murine neural progenitors elicits benign neoplasms composed of enlarged dysmorphic neurons and neoplastic astroglia recapitulating ganglioglioma (GG) only in concert with active Akt/mTOR-signaling. Purely glial tumors resembling aspects of polymorphous low-grade neuroepithelial tumors of the young (PLNTYs) emerge from *BRAF^V600E* alone. Additional somatic *Trp53*-loss is sufficient to generate anaplastic GGs (aGGs) with glioneuronal clonality. Functionally, only *BRAF^V600E*/*p*Akt tumors intrinsically generate substantial neuronal activity and show enhanced relay to adjacent tissue conferring high epilepsy propensity. In contrast, PLNTY- and aGG models lack significant spike activity, which appears in line with the glial differentiation of the former and a dysfunctional tissue structure combined with reduced neuronal transcript signatures in the latter.

Conclusion. mTOR-signaling and *Trp53*-loss critically determine the biological diversity and electrical activity of *BRAF^V600E*-induced tumors.

Key Points

- IUE of *BRAF^V600E* and activation of mTOR leads to ganglioglioma (GG)-like tumors, while *BRAF^V600E* alone gives rise to PLNTY-like neoplasms.
- Anaplastic GGs depend on the *Trp53* deletion in combination with *BRAF^V600E* and Akt/mTOR-signaling cascade.

Activating *BRAF^V600E* somatic mutations have been detected in different developmental low-grade glial and glioneuronal brain tumors.[1–5] *BRAF^V600E* is particularly frequent in up to approximately 60% of gangliogliomas (GGs) and has been observed in both dysmorphic neuronal and neoplastic astroglial tumor cells.[6] GGs are typical pediatric neoplasms

Importance of the Study

Glioneuronal tumors are challenging with respect to biological behavior and seizure emergence. While *BRAF^V600E^* in murine neural precursors induces oligoid tumors, it requires an overactivation of Akt/ mTOR-signaling for the development of hyperexcitable gangliogliomas and additional *Trp53*-loss for anaplastic transformation.

and represent the most frequent tumor entity in patients undergoing epilepsy surgery.[7,8] Intraventricular in utero electroporation (IUE) of the murine *BRAF^V600E^* equivalent (*Braf^V637E^*) during early brain development induced cyto-architectural abnormalities of mutant neurons, increased numbers of astro- and oligodendroglia, and seizures in mutant mice.[9]

However, *BRAF^V600E^* is present in a large variety of purely glial neoplasms including polymorphous low-grade neuro-epithelial tumors of the young (PLNTY)[5] and glioneuronal tumors with distinct malignancies and seizure propensities. Molecular factors conferring this heterogeneity are unresolved. Recent reports have suggested that the Akt/mTOR-pathway is activated in humans, *BRAF^V600E^*-positive GGs.[10–13] Despite the fact that most GGs behave biologically benign, anaplastic variants (aGGs) occur, representing onco- and epileptological challenges. The significance of *Trp53* mutations has remained controversial for human aGGs.[14–16] Recently, *Trp53* mutations were reported as prognostically relevant for seizure control in human aGGs.[17]

Here, we have scrutinized in IUE-induced somatic *BRAF^V600E^*-positive murine developmental brain tumors, whether active Akt/mTOR-signaling mediated through constitutively phosphorylated Akt kinase (*p*Akt) as well as *Trp53*-loss confers heterogeneity to resulting tumors. Furthermore, we have analyzed whether the emerging neoplasms manifest with distinct electrical activity.

Materials and Methods

Patient Samples

*BRAF^V600E^*-positive tumor biopsies were from the University of Bonn Medical Center Neurosurgery Program. All procedures were conducted in accordance with the Declaration of Helsinki and approved by the Local Ethics Committee.

Molecular and Cellular Approaches

IUE of pBase together with piggyBac transgenes were injected into the lateral ventricle of mouse embryos at embryonic day 14 (E14) (see Supplementary Materials and Methods). All experiments involving animals were performed in accordance with the guidelines of the Medical Faculty, University of Bonn, Animal Care Committee and the guidelines approved by the European Directive (2010/63/EU) and ARRIVE. Histological and immunohistochemical approaches are described in detail

in the Supplementary Materials and Methods. For RNA sequencing (RNA-seq) experiments, library preparation was performed using QuantSeq 3′-mRNA-Seq Library Prep kit (Lexogen) and subjected on a HiSeq 2500 sequencer (Illumina) with 1 × 50 bp single-end reads and a coverage of 10 000 reads per sample. The RNA-seq data have been deposited in the Gene Expression Omnibus (GEO) database (accession number GSE18072).

Electrophysiological Recordings

Acute brain slices were measured on a 64-electrode multielectrode array (MEA) plate (8 × 8 grid, each with a diameter of 50 μM; see Supplementary Materials and Methods).

Statistical Analysis

Statistical analysis and graphs were performed using GraphPad Prism, Igor 64, and RStudio. All results are plotted as ±SEM and *P*-values were indicated as $*P < .05$, $**P < .01$, $***P < .001$, $****P < .0001$.

Results

*BRAF^V600E^*-Induced Tumor Characteristics Determined by Akt/mTOR-Pathway Activation

The spectrum of *BRAF^V600E^*-positive tumors comprises glioneuronal/GG and glial/PLNTY entities (Figure 1A and B). We observed the phospho-ribosomal protein S6 (*p*S6) as downstream effector of Akt/mTOR-pathway signaling to be present in GGs (Figure 1A, n = 3)[13] but virtually absent from PLNTYs (Figure 1B, n = 5). It is so far unresolved, whether Akt/mTOR-pathway activity with its surrogate marker *p*S6 is relevant for the emergence of glioneuronal lesions or for example, a consequence of frequently associated epileptiform activity.[13,18] To address this topic, we have developed mouse models based on the manipulation of *BRAF^V600E^* and Akt/mTOR-pathway signaling for which we first analyzed key molecular mediators of the Akt/mTOR-pathway in vitro. RAS/ERK signaling has been reported to site-specifically phosphorylate ribosomal protein S6 and *BRAF^V600E^* has been demonstrated to induce phosphorylation of S6 at S235/6 in HEK293T cells.[19,20] Whereas *BRAF^V600E^* alone did not result in increased phosphorylation of S6 and 4E-BP1 in cultured neural cells, co-expression of constitutively active lyn-Akt (further referred to as *p*Akt) induced significantly increased phosphorylation of S6 at
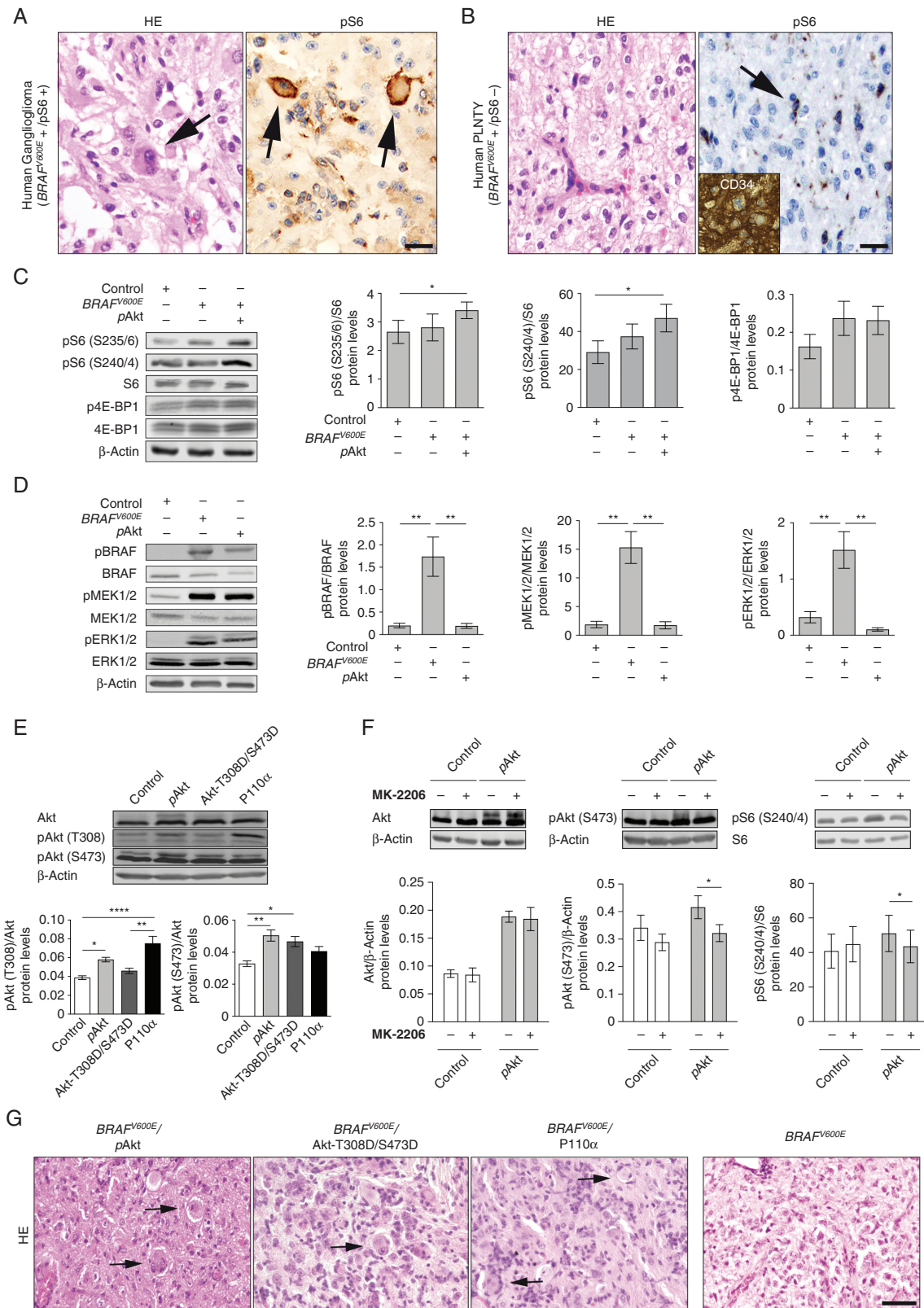
Fig. 1 mTOR-pathway activation in human GGs and in-vitro assessment of *p*Akt potential to activate the mTOR-pathway. (A) Representative human GG harboring dysplastic neurons positive for *p*S6 (arrows) vs (B) PLNTY contains prominent monomorphic oligoid cells, negative for *p*S6

both S235/6 and S240/4 sites (Figure 1C; Supplementary Figure S5). There were no parallel effects on the phosphorylation status of 4E-BP1 (Figure 1C; Supplementary Figure S5). Immunoblot analyses further revealed efficient phosphorylation of several main downstream targets by *BRAF^V600E* including BRAF, ERK1/2, and MEK1/2 (Figure 1D). Only lyn-Akt significantly increased Akt phosphorylation at both T308 and S473 sites in vitro, whereas neither Akt-T308D/S473D nor overexpression of the PI3K catalytic subunit P110α[21] induced parallel effects (Figure 1E; Supplementary Figure S6). Additionally, pharmacological experiments with MK-2206, an allosteric inhibitor of Akt, significantly decreased phosphorylation of Akt and S6 following *p*Akt expression (Figure 1F).

Next, we performed IUE in mice with the piggyBac transposon system (pBase) (Supplementary Figure S1A).[22] Intriguingly, co-IUE of *BRAF^V600E* with either *p*Akt, Akt-T308D/S473D or overexpression of P110α resulted in tumors harboring enlarged, sometimes binucleated dysmorphic neurons, intermingled with process-rich astroglial cells (n = 5; Figure 1G). All animals IU-electroporated with *BRAF^V600E* only (1-hit model; Supplementary Figure S1D) developed circumscribed lesions composed of oligoid cells (n = 8; Figure 1G). *BRAF^V600E* mice further showed strong expression of the oncofetal protein CD34 within the *BRAF^V600E* tumor region (Supplementary Figure S2). Thus, these tumors recapitulated the main neuropathological aspects of PLNTYs. None of the control animals (n = 8; Supplementary Figure S1B) developed any tumors. IUE of only *p*Akt (Supplementary Figure S1C) did not result in detectable tumors until P110 (data not shown; n = 6).

The combination of *BRAF^V600E* and *p*Akt (further designated as *BRAF^V600E*/*p*Akt or 2-hit model; Supplementary Figure S1E) strongly resemble core features of human GGs.[10–13] Thus, we focused on this model in the further experiments. We next analyzed key molecular and cellular characteristics of *BRAF^V600E*/*p*Akt-induced tumors and compared them to neoplasms emerging from *BRAF^V600E* alone. *BRAF^V600E*/*p*Akt IU-electroporated mice showed strong *p*S6 expression (Figure 2B and C), as well as phosphorylation of the downstream ERK1/2 protein (Figure 2D and E) indicating robust activation of Akt/mTOR-pathway signaling in these tumors. Subsequent immunofluorescence analysis revealed a glioneuronal phenotype composed of enlarged dysmorphic neuronal-shaped cells positive for the microtubule-associated protein 2 (MAP2) interspersed in a dense glial fibrillary acidic protein (GFAP)-positive matrix in the 2-hit tumors (Figure 2F, upper panels). In contrast, 1-hit neoplasms contained MAP2-positive cells with a monomorphic shape and only few nonneoplastic, thus reactive GFAP-positive astrocytes (Figure 2F, lower panels). Additional co-immunolabeling analyses demonstrated co-localization between GFAP and mCherry-IU-electroporated cells in 2-hit tumors (Figure 2G, upper panels). Furthermore, we observed mCherry-IU-electroporated cells positive for nuclear Ki-67 expression (Supplementary Figure S3), suggesting a neoplastic astroglial component. Contrarily, the lack of mCherry-IU-electroporated cells positive for GFAP in 1-hit neoplasms identified GFAP-positive cells as reactive astrocytes (Figure 2G, lower panels and Supplementary Figure S3). *BRAF^V600E*/*p*Akt-mCherry, but not *BRAF^V600E*-targeted cells, co-localized with the neuron-specific nuclear protein NeuN, indicating their neuronal phenotype (Figure 2H). Both 1- and 2-hit tumors revealed mCherry- and oligodendrocyte transcription factor 2 (Olig2)-positive tumor cells (Figure 2I). Olig2 expressing oligoid-shaped cells recapitulated key features of human PLNTY.[5] Thus, *BRAF^V600E* alone in E14 neural progenitors elicits tumors with oligodendroglial, thus PLNTY-like features, whereas in concert with robust Akt/mTOR-pathway signaling glioneuronal neoplasms recapitulating GG features emerge. *p*Akt-induced Akt/mTOR-pathway signaling acts as nonneoplastic but phenotypically modifying factor of *BRAF^V600E*-induced tumors. Of note, 1- and 2-hit tumors lacked augmented mitotic figures and thus appeared benign.

Anaplasia of *BRAF^V600E*/*p*Akt-Induced Tumors Through *Trp53*-Loss

In GGs, anaplasia of the astroglial component is an enigmatic issue[23] and the significance of anaplastic histological features in GGs for patient survival has remained controversial.[24,25] The pathogenetic impact of loss-of-function *Trp53* mutations in human aGGs is unresolved.[15,26] To study this aspect, we have modified the 2-hit model by co-IU-electroporating *BRAF^V600E*, *p*Akt, and Cre at E14 in *Trp53^loxP/loxP* mice (further designated as *BRAF^V600E*/*p*Akt/*Trp53^KO* or 3-hit model; Supplementary Figure S1F). *BRAF^V600E*/*p*Akt/*Trp53^KO* introduced into neural progenitors resulted in diffusely infiltrating tumors with high cellularity and Ki67-labeling index of the astroglial, thus neoplastic malignant component (n = 19; Figure 3A and B). The tumors retained GG features by the presence of large, dysmorphic neurons (Figure 3B and C). The astroglial tumor

---

Fig. 1, continued

(arrow; scale bar, 100 μm) and positive for CD34 (inset; scale bar, 50 μm). (C) Representative immunoblots and quantification of *p*S6 (S235/6)/S6, *p*S6 (S240/4)/S6, and p4E-BP1/4E-BP1 protein levels after transfection of NS20Y cells with Control, *BRAF^V600E*, and *BRAF^V600E*/*p*Akt plasmids (n = 4). (D) Immunoblots and quantification of pBRAF/BRAF, pERK/ERK, and pMEK1/2/MEK1/2 for Control, *BRAF^V600E*, and *p*Akt conditions (n = 5). (E) Representative immunoblots of Akt, Akt (T308), and Akt (S473) from Control-, *p*Akt-, Akt-T308D/S473D-, and P110α-transfected NS20Y protein lysates and quantification of *p*Akt (T308)/Akt and *p*Akt (S473)/Akt protein levels (n = 5). One-way ANOVA followed by Tukey's multiple comparison test. (F) Treatment with MK-2206 after transfection with Control or *p*Akt and corresponding quantification of Akt, *p*Akt (S473), and *p*S6 (S240/4) protein levels in NS20Y cells (n = 4). Two-way ANOVA followed by Sidak's multiple comparison test. An antibody against β-actin was used as loading control in all cases. (G) H&E-stained sections of *BRAF^V600E*/*p*Akt, *BRAF^V600E*/Akt-T308D/S473D, *BRAF^V600E*/P110α (2-hit)-, and *BRAF^V600E* (1-hit)-IUE brains (>P40). Arrows point to dysmorphic neurons in *BRAF^V600E*/*p*Akt model. Scale bar, 25 μm. Abbreviations: GG, ganglioglioma; H&E, hematoxylin and eosin; IUE, in utero electroporation; PLNTY, polymorphous low-grade neuroepithelial tumors of the young.
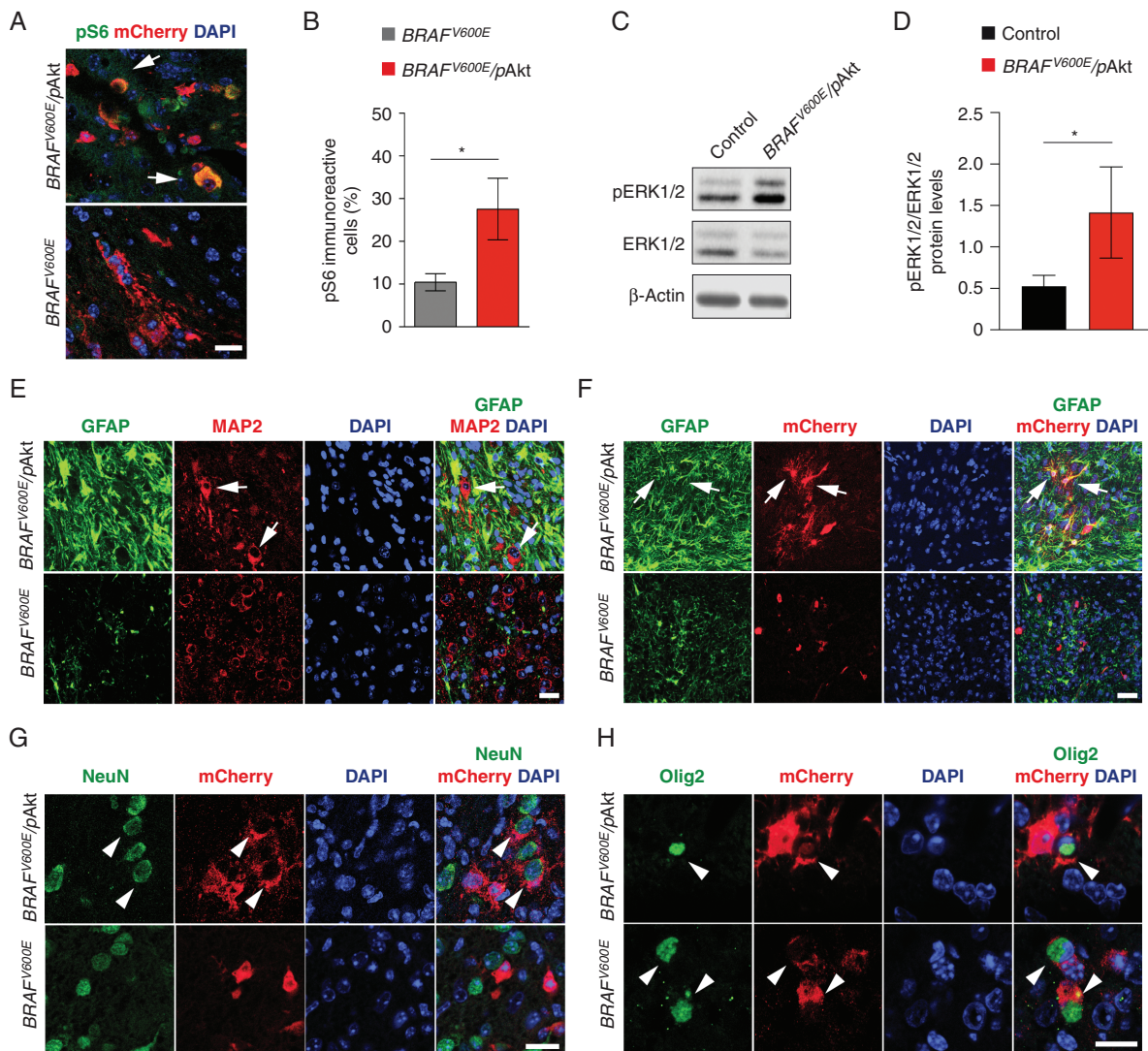
Fig. 2 Level of mTOR-pathway activation fundamentally impacts *BRAF*^{V600E}-induced tumors characteristics. (A) CD34 immunolabeling of *BRAF*^{V600E} tumors. Scale bars, 330 μm (left panel) and 30 μm (right panel). (B) Expression of *p*S6 in *BRAF*^{V600E} and *BRAF*^{V600E}/*p*Akt-induced tumors. Arrows point to *p*S6-positive mCherry cell in *BRAF*^{V600E}/*p*Akt tumor (n = 5). Scale bar, 25 μm. (C) Quantification of *p*S6-immunoreactive cells in the 2- vs 1-hit tumors (n = 5). Two-tailed unpaired *t*-test. (D) Representative immunoblots of *BRAF*^{V600E}/*p*Akt tumor and control NS20Y protein lysates of pERK1/2 and ERK1/2 detected by Western blot. (E) Quantification of the expression levels of pERK1/2/ERK1/2 protein levels from *BRAF*^{V600E}/*p*Akt tumor compared to control (n = 5). β-Actin was used as loading control. Ratio paired *t*-test. (F) *BRAF*^{V600E}/*p*Akt-induced tumors reveal an admixture of large dysplastic MAP2-positive neurons (white arrows) and a dense GFAP-positive astroglial matrix. 1-hit model tumors are composed of small isomorphic MAP2-positive elements. (G) Immunofluorescent labeling of GFAP by a fraction of mCherry-positive cells in *BRAF*^{V600E}/*p*Akt tumors (white arrows) and the absence of GFAP-positive tumor cells in 1-hit tumors. (H) NeuN- and mCherry (*BRAF*^{V600E}/*p*Akt)-positive large neurons in the 2-hit model (white arrowheads) vs small and circular shaped mCherry-positive but NeuN-negative cells in the 1-hit model. (I) Co-expression of Olig2 and mCherry in both 1- and 2-hit model tumors (white arrowheads). Scale bars, 25 μm. Abbreviations: GFAP, glial fibrillary acidic protein; MAP2, microtubule-associated protein 2.

component appeared malignant due to high pleomorphism, density, and proliferation (Figure 3D, arrows). Of note, IUE of only Cre at E14 in *Trp53*$^{loxP/loxP}$ mice did not result in any emerging tumors (n = 5; data not shown). Thus, *Trp53*-loss does not elicit aGG-like tumors independently from *BRAF*^{V600E}/*p*Akt, but in the present context clearly acts as a modifier that leads to the acquisition of anaplastic tumor features.

Glioneuronal Clonality of *BRAF*^{V600E}/*p*Akt/*Trp53*^{KO} Cell Populations

Particularly for aGGs, the glioneuronal character has been questioned due to the fact that the glial tumor fraction recapitulates malignant features resembling glioblastoma multiforme such that dysmorphic neurons and neoplastic astroglia might derive from different rather than identical
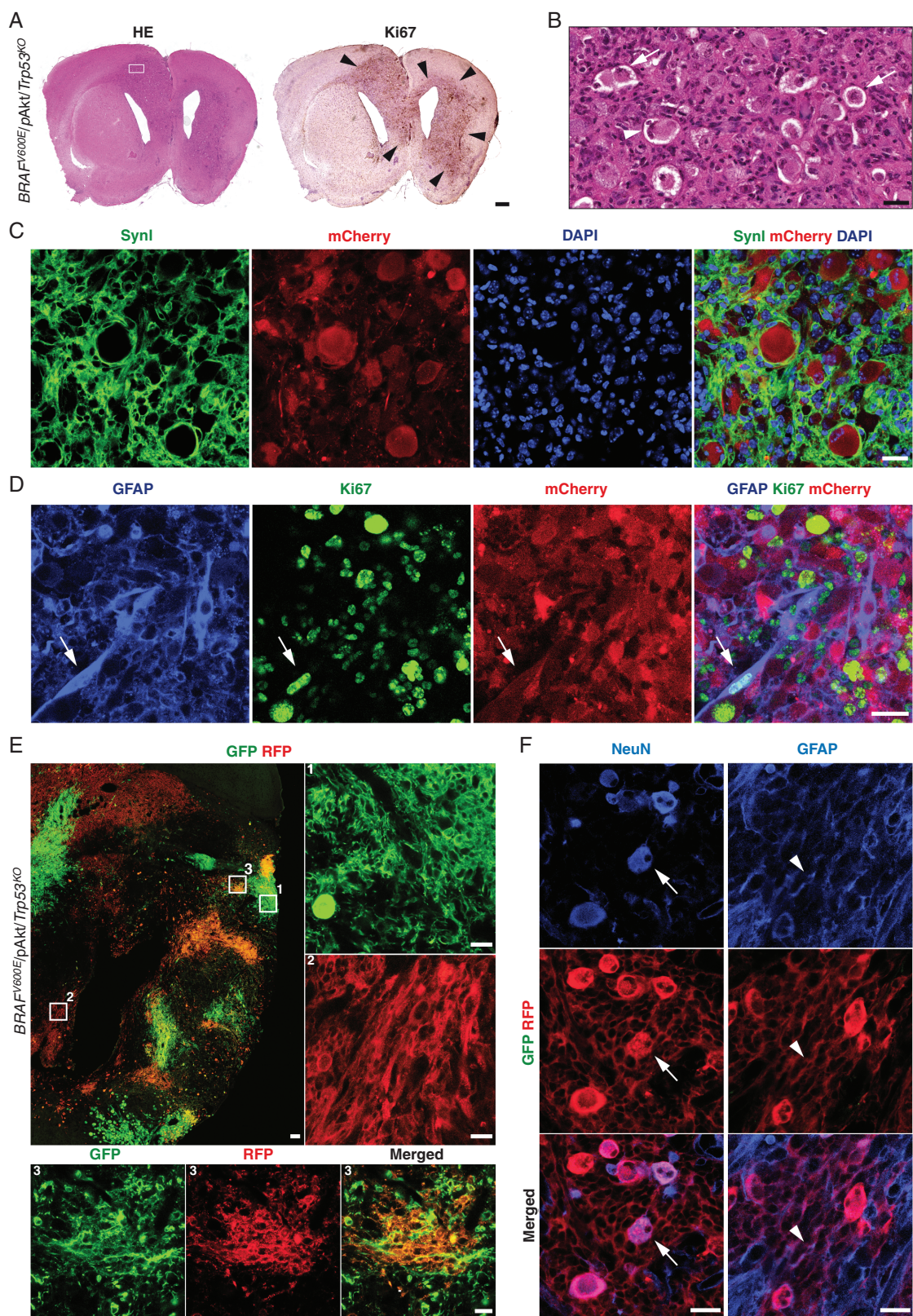
Fig. 3 Anaplastic phenotype and clonal architecture through *Trp53*-loss in developmental *BRAF^{V600E}*/pAkt-induced tumors. (A) Coronal view of a *BRAF^{V600E}*/pAkt/*Trp53^{KO}* mouse brain (P40) harboring a large hemispheric tumor with prominent mass effect (H&E staining) and corresponding immunostaining against the proliferation-related antigen Ki67 (arrowheads); scale bar, 500 μm. (B) Enlarged area of the tumor

precursor cells. To address this issue, we used a genetic cell labeling technique that generates different hues by combinatorial and stochastic expression of few distinct fluorescent proteins, enhanced green fluorescent protein (eGFP), mOrange, and mKate2 creating multicolor clonal labeling (Brainbow 3.0 allele cloned under the control of a constitutive promoter into the piggyBac plasmid Supplementary Figure S4A).[27,28] We next IU-electroporated the piggyBac-Brainbow construct when eliciting 3-hit model tumors (n = 5; further designated as *BRAF^{V600E}/pAkt/Trp53^{KO}/Brainbow*; Supplementary Figure S4D). Multicolor labeling of tumor cells at P20 allowed the visualization of tumor cell clonality (Figure 3E). The intermingled distribution of differently colored astroglia indicates parallel clonal expansion and mixing of tumor cells (Figure 3E). Overall, distinct colors were always labeling neurons (representative images Figure 3F, left panels) and astroglia (representative images Figure 3F, right panels), indicating that the present IUE generally hits glioneuronal progenitor cells enforced by the genetic manipulation to give rise to both dysmorphic neuronal and glial tumor cell fractions and argues against an ontological concept of GGs-based tumorigenesis by neoplastic transformation of astroglia within a dysplastic precursor lesion. Thus, dysmorphic neurons and malignant astroglia both represent tumor components of the 3-hit neoplasms.

Growth Dynamics and Survival Kinetics Reflect Tumor Genetics

Concerning biological behavior, both 1- and 2-hit models revealed favorable survival kinetics (n = 8, with 87.5% of the mice still being alive at the age of P110 for *BRAF^{V600E}*-positive tumors, 88.9% survival at P110 (n = 9) for *BRAF^{V600E}/pAkt*-positive tumors; Figure 4A) and very low Ki67-labeling proliferation indices (Figure 4B). In contrast, anaplastic histological features of 3-hit tumors were reflected by poor survival up to only P70 (n = 19; Figure 4A) and an extensively increased Ki67-immunoreactive index (Figure 4B).

Despite the fact that differences in survival rate and proliferation of the tumor models indicate distinct biological behavior, we aimed to analyze in vivo whether different molecular architectures substantially impact tumor growth kinetics by IUE of plasmid coding for the near-infrared fluorescent protein (iRFP713). In-vivo near-infrared imaging at P10, P20, and P45 allowed to follow growth dynamics in the individual tumor models (Figure 4C). Intriguingly, *BRAF^{V600E}*-positive neoplasms apparently represent early developmental tumors since the growth dynamics were apparently exhausted already at P10 (Figure 4C). The initial oncogenic stimulus mediated by the mutant *BRAF^{V600E}*

variant may rapidly convert into oncogene-induced interruption of proliferation and differentiation as tumor-related phenomenon that parallels previous observations coined "*BRAF^{V600E}*-induced senescence" in human neural stem cells and progenitors.[29] In contrast, 2-hit tumors preserved growth dynamics for a longer time period until P20, whereas in mice harboring 3-hit tumors, dynamic expansion even remained present throughout the entire observational period (Figure 4C).

Next, we cultured 3-hit tumor cells in vitro (Figure 4D). Re-expression of *Trp53* under control of the ubiquitous elongation factor 1 alpha (Ef1α) promoter 7 days after transduction lead to significantly reduced cell viability (Figure 4E). Thus, wild-type p53 can induce tumor cell degeneration even in the molecular context of multiple tumor-promoting genetic alterations. Selective inhibition of the MAPK- and mTOR-signaling cascades in *BRAF^{V600E}/pAkt/Trp53^{KO}* tumor cells by vemurafenib and rapamycin both resulted in reduced cell viability (Figure 4F and I), a sustained blockage of tumor cell proliferation over time (Figure 4G and J) and reduced *p*MEK1/2, relative to MEK1/2 protein levels for vemurafenib and reduced *p*S6, relative to S6 protein levels for rapamycin (Figure 4H and K). Interfering with either MAPK- or mTOR-signaling fundamentally thus decreases tumor cell viability.

RNA Signatures Indicate Impaired Neuronal Signaling and Increased Invasive Glial Growth in *BRAF^{V600E}/pAkt/Trp53^{KO}* Tumors

Next, we pursued to understand whether 3-hit tumors would recapitulate transcript features of high-grade gliomas or glioneuronal tumors[9,30,31] or alternatively integrate characteristics of both, thereby creating a unique RNA fingerprint. RNA-seq of *BRAF^{V600E}/pAkt/Trp53^{KO}* tumor and gray-/white matter matched control (ctrl) tissue (n = 4 per group; P40) identified abundant genes to be differentially expressed (3141 genes in- vs 2700 genes decreased in expression in tumor tissue; Figure 5A). Principal component analysis (PCA) of the RNA-seq data clearly separated the 3-hit tumors from control tissue samples (Figure 5B). Intriguingly, gene ontology (GO) enrichment analysis revealed that the term with the most pronouncedly induced signature in fact relates to inflammation and is accompanied by augmented transcripts with biological functions that reflect malignant glioma characteristics including proliferation, invasion, and neovascularization (Figure 5C). Transcripts reduced in tumor tissue grouped under GO terms related to neuronal homeostasis and signal transduction (Figure 5C). This observation rather reflects true expression regulation rather than simply different tissue composition between tumor and control

Fig. 3, continued
shown in A (square) demonstrates the presence of dysmorphic (arrows), occasionally binucleated (arrowhead) neurons in an astroglial matrix with high cellularity and pleomorphism. (C) Immunofluorescence confirms the SynI-positive neurons as mCherry-positive tumor components. (D) The GFAP-/mCherry-positive astroglial tumor cell component (white arrows) reveals a high fraction of Ki67-expressing elements as sign of anaplasia. (E) Representative section of a *BRAF^{V600E}/pAkt/Trp53^{KO}/Brainbow* tumor at P20 (n = 5). Scale bar, 100 μm. Right and low panels show high magnification images of white squares 1, 2, and 3 from the overview image. (F) Neurons (arrows; NeuN-immunohistochemistry) and astroglial (arrowheads; GFAP-immunohistochemistry) cells in a brainbow red fluorescent protein (RFP)-labeled tumor clone. Scale bars, 25 μm. Abbreviations: GFAP, glial fibrillary acidic protein; H&E, hematoxylin and eosin.
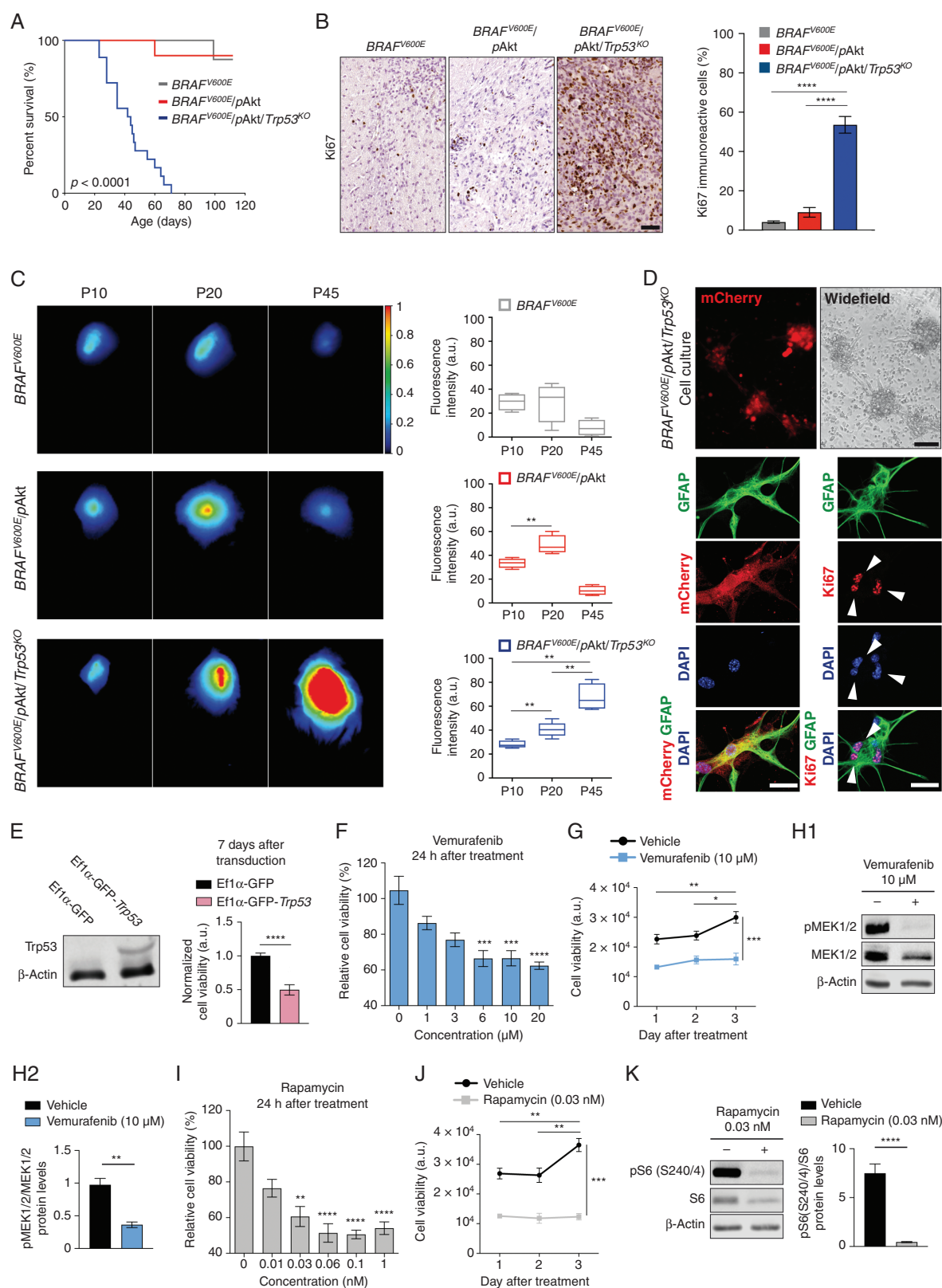
Fig. 4 Distinct in-vivo growth kinetics of GG models. (A) Kaplan-Meier survival curves of mice IU-electroporated at E14 with *BRAF^{V600E}* (*gray* line, n = 8); *BRAF^{V600E}*/*p*Akt (*red* line, n = 9); and *BRAF^{V600E}*/*p*Akt/*Trp53^{KO}* (*blue* line, n = 19). Log-rank test. (B) Representative pho-tomicrograph of Ki67-stained brain sections for the different tumor models. Percentage of proliferating, neoplastic cells within the tumor area

samples since a significant portion of neuronal transcripts was unchanged or even increased between tumor and control tissue (Supplementary Table S2). Heat map clustering revealed an overall lower expression of distinct families of channels and receptors (Figure 5D). In each family, only sets of transcripts showed robustly reduced transcript patterns whereas other subunits were unchanged in tumor tissue (Figure 5E–J). Considering the particular morphological and molecular features of the aGG model, we aimed to understand whether these tumors differ from low-grade *BRAF^V600E*-induced neoplasms in functional, excitability-related terms.

Electrical Activity Patterns Differentiate *BRAF^V600E*-Tumor Variants

BRAF^V600E-positive/glioneuronal tumors are particularly epileptogenic and altered neuronal activity in tumor microenvironmental (TME) networks has been recently demonstrated also in malignant gliomas.[9,32–34] We sought to analyze systematically whether differences in intrinsic excitability as well as TME neuronal networks occur in the different *BRAF^V600E*-positive tumors under study and, therefore, tested electrical activity in acute brain slices containing the tumor at P50-60 using a MEA system. Based on the distribution of mCherry-positive cells, electrodes were classified into three categories: (i) IUE Tumor core (area with mCherry-positive tumor cells), (ii) peri-IUE (tumor border), and (iii) nonfluorescent tissue (preexisting brain tissue) (Figure 6A and B). Extracellular activity was recorded by the 64 electrodes of the MEA plate, encompassing the three different categories (Figure 6C). Similar to previous results from low-grade human gliomas,[32] the lowest frequency of spontaneous activity was observed for all models in the tumor core (Figure 6D). Spontaneous spike activity from slices incubated with artificial cerebrospinal fluid (aCSF) could clearly be resolved within the three different categories and in all groups (Figure 6D and E) and at frequencies comparable to control in the peri-tumoral area and the surrounding tissue (Figure 6F, *yellow* and *blue* bars). However, groups significantly differed in the number of spikes produced per area in the tumor core region: only *BRAF^V600E*/*p*Akt tumors displayed activity at levels not different to controls whereas both *BRAF^V600E* only and *BRAF^V600E*/*p*Akt/*Trp53^KO* appeared almost silent in this central region (*red* bars).

As brain slices are an isolated preparation lacking any sensory input, levels of neuronal activity are much lower than in vivo. To probe how the distinct tumor entities responded to elevated activity, we recorded spikes in brain slices bathed in a solution favoring network activity (aCSF low Mg^{2+}, high K^+). This maneuver could not increase activity in the tumor core regions of all three models (except for the control group) (Figure 6G, *red* bars), suggesting that the central cytoarchitecture in the *BRAF^V600E* and *BRAF^V600E*/*p*Akt/*Trp53^KO* neoplasms does not allow regular neuronal firing and that also in the *BRAF^V600E*/*p*Akt tissue the dynamic range of neuronal activity is compromised compared to control. *BRAF^V600E* and *BRAF^V600E*/*p*Akt/*Trp53^KO* tumors in the peri-tumoral area also did not respond to the solution exchange and thereby dampen activity infiltrating this region. Strikingly, we observed that activity was substantially amplified in this transitional zone in *BRAF^V600E*/*p*Akt mice and even exceeded the level of increase seen in control mice (Figure 6G, *yellow* bars). Together with ongoing spontaneous activity in the core region, this suggests that the *BRAF^V600E*/*p*Akt tumor model exhibits the strongest epileptogenic propensity.

Discussion

Despite representing a seminal discovery, the presence of *BRAF^V600E* as prominent somatic mutation in developmental brain tumors demands further explanation with respect to (a) the large variety of affected glial and glioneuronal entities, including PLNTY and GGs[3,5] and (b) differences in their biological behavior with a controversial role of *Trp53*.[14–17,35] Our present data indicate that the heterogeneity and excitability of *BRAF^V600E*-induced murine developmental brain tumors critically depend on the activity status of Akt/mTOR-pathway signaling and that *Trp53*-loss has fundamental impact on the acquisition of malignant features.

Only *BRAF^V600E* on its own but not *p*Akt or *Trp53*-loss revealed the potential to induce neoplasia (Supplementary Table S1). Thus, *BRAF^V600E* represents the primary oncogenic driver, whereas *p*Akt and loss of *Trp53* confer specific pathogenetic and functional tumor features. Augmented Akt/mTOR-pathway signaling in concert with *BRAF^V600E* appears as precondition for the acquisition of glioneuronal features with frank dysmorphic neurons and neoplastic astroglia in emerging neoplasms reflecting human GGs.[13]

Fig. 4, continued

(N = 3-5; n = 10). (C) Representative in-vivo iRFP brain tumor signals of 1-, 2-, and 3-hit tumor mice were detected at P10, P20, and P45 (color bar—total fluorescence efficiency in pseudo-color). Quantification of iRFP signals of the different tumor variants (n = 4-6). Regions of interest (ROIs) were defined above the tumor region and the fluorescence intensity was defined in arbitrary units (a.u.). One-way ANOVA followed by Tukey's multiple comparison test. (D) Representative images of *BRAF^V600E*/*p*Akt/*Trp53^KO*-derived cultured cells at day 7 in vitro (upper panels; scale bar, 100 μm) and immunohistochemistry against mCherry, GFAP, and Ki67 (lower panels; scale bar, 25 μm). (E) Western blot of *Trp53* from *BRAF^V600E*/*p*Akt/*Trp53^KO* tumor cells transduced with lentiviruses expressing Ef1α-GFP or Ef1α-GFP-*Trp53*. Graph bar represents normalized levels of cell viability of *BRAF^V600E*/*p*Akt/*Trp53^KO* 7 days after transduction (n = 3). Mann-Whitney *U* test. (F, I) Relative cell viability of *BRAF^V600E*/*p*Akt/*Trp53^KO* tumor cells after 24-h exposure with increasing concentrations of vemurafenib (F) and rapamycin (I). Kruskal-Wallis test followed by Dunn's multiple comparison test. (G, J) Time-dependent viability of cells treated with vemurafenib (G) and rapamycin (J). Two-way ANOVA followed by Sidak's multiple comparison test. (H, K) Representative Western blot and quantification of pMEK1/2/MEK1/2 (H) and *p*S6 (Ser240/4)/S6 (K) ratios from cell protein lysates following vemurafenib (H) and rapamycin (K) treatments. β-Actin was used as loading control (n = 3). Unpaired *t*-test. Abbreviations: GFAP, glial fibrillary acidic protein; GG, ganglioglioma; iRFP, near-infrared fluorescent protein.
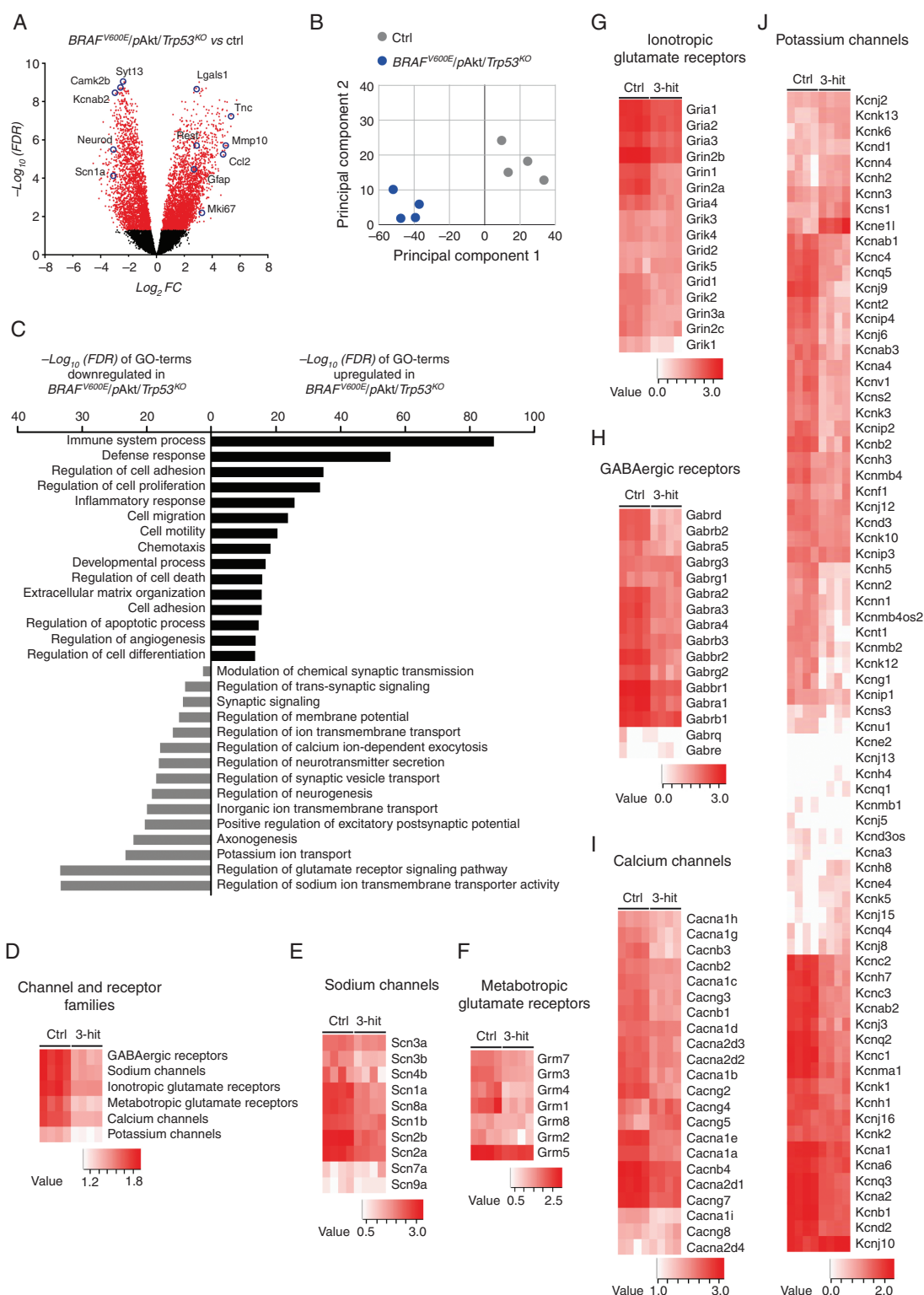
Fig. 5   Transcriptomic analysis of *BRAF*^{V600E}/*p*Akt/*Trp53*^{KO}-induced tumors reveals malignant glial and non-homeostatic neuronal signatures. (A) Volcano plot represents differentially expressed genes (5842) in 3-hit tumors compared to gray/white matter matched control (ctrl) tissue (n = 4). Each gene is colored based on the −log$_{10}$ adjusted *P*-value (false discovery rate [FDR]). *Red* dots: FDR < 0.05: *black* dots: FDR > 0.05. (B) PCA plot clearly separates 3-hit tumors (*blue* dots) from controls (*gray* dots); transcript signatures of four biological replicates. (C) Gene ontology (GO) terms based on significantly enriched genes from 3-hit tumors compared to control tissue. (D–J) Heatmap visualizations of expression levels of genes coding for synaptic-related channels and receptors. Abbreviations: PCA, principal component analysis.
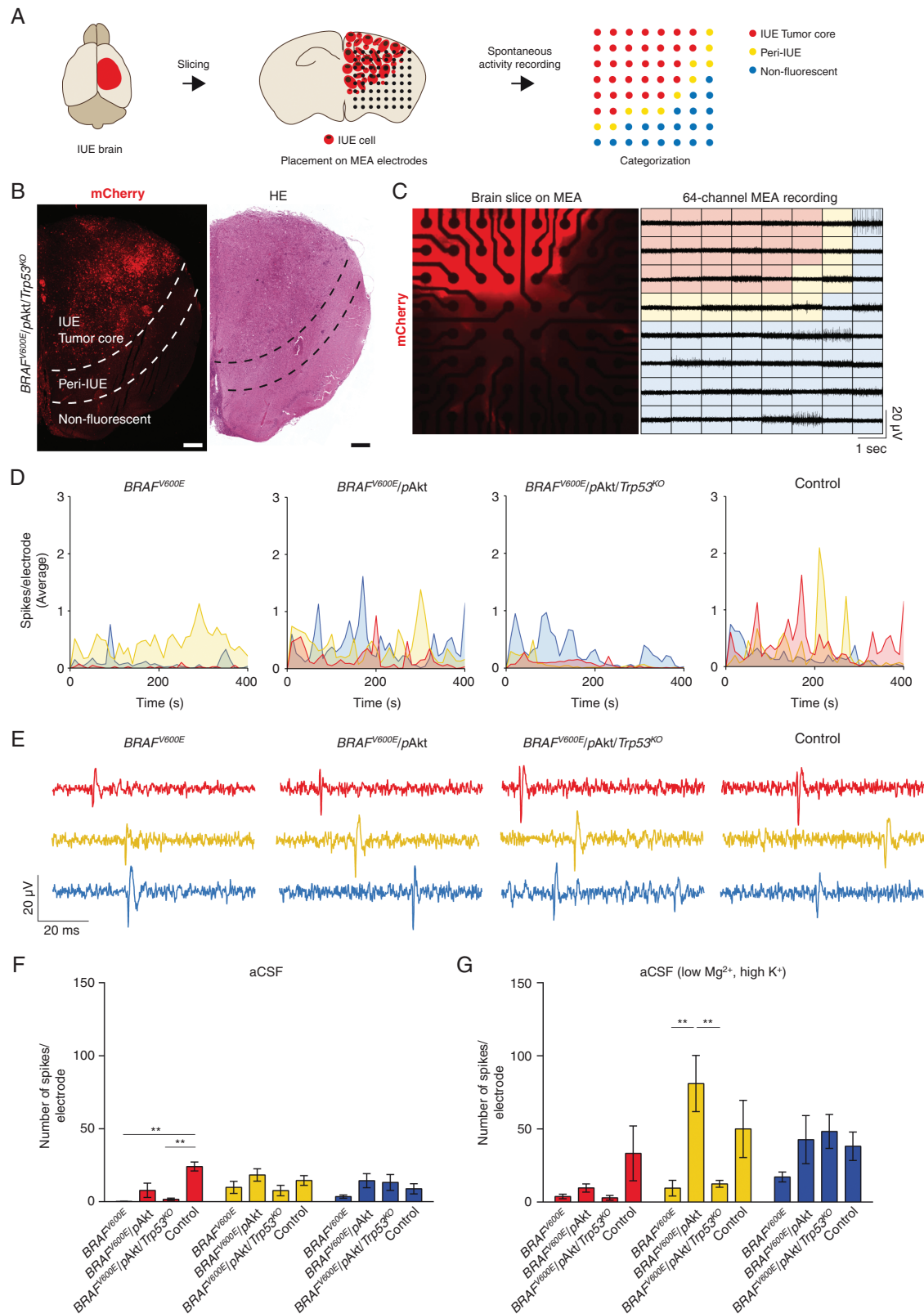
Fig. 6 MEA-based recordings of spontaneous neuronal activity of murine GG brain slices. (A) Scheme of the experimental workflow. (B) Overview of a coronal slice of a *BRAF*[V600E]/*p*Akt/*Trp53*[KO] brain. Scale bar, 500 μm. (C) *BRAF*[V600E]/*p*Akt/*Trp53*[KO] tumor slice on the MEA grid consisting of 64 electrodes visualized by the mCherry expression (left panel). Right panel: extracellular voltage signal traces. (D) Time-dependent

In contrast, *BRAF*^{V600E} alone introduced to neural pre-cursors at E14 elicited MAP2-/Olig2-positive oligoid tumors that histologically resemble key cellular aspects of PLNTY, further supported by strong CD34 positivity. In two human series, oligodendroglial features and the presence of either *BRAF*^{V600E} or mutually exclusive fusion events involving FGFR2/FGFR3 were reported for PLNTY.[5,36] Different molecular modifications converge in activating MAPK signaling. Of note, glioneuronal lesions have been demonstrated to arise from embryonal IUE-mediated transfer of GLAST-*BRAF*^{V600E} and Nestin-*BRAF*^{V600E}, respectively,[30] and in *BRAF*^{V637E}-transgenic mice virally injected with episomal Cre plasmid (Supplementary Table S1).[9] Thus, the particular progenitor target subpopulation and the distinct developmental timepoint of somatic mutation may further increase the heterogeneity of *BRAF*^{V600E}-induced tumors.

A further difference of the models applied in our present study is given by the use of a truncated *BRAF*^{V600E} containing kinase domain. Truncated *BRAF*^{V600E} introduced by retroviral vector into neonatal Ntv mice under control of the Nestin promoter-induced tumors resembling pilocytic astrocytoma.[37] In contrast, full-length *BRAF*^{V600E} did not exert effects. This may be due to increased negative regulation of BRAF activity through a potential phosphorylation of inhibiting residues in the C-terminal domain in progenitor pool available at birth or through Hsp90 stabilizing binding in the full-length *BRAF*^{V600E} protein.[38] Even though *BRAF*^{V600E} has been reported to activate mTOR-pathway signaling,[20] the present data argue for further phosphorylation of Akt as requirement for the downstream activation of S6 but not 4E-BP1 concomitant with the development of tumors recapitulating key GG features. Abundant phosphorylation of both sites of *S6*, Ser235/236, and Ser240/244, has been in fact independently related to key characteristics of dysmorphic neurons, including hypertrophism as well as severely impaired dendritogenesis.[39,40] Of note, considering that glioma formation through mTOR activation via Nf1 is independent of TSC1/2/Rheb mechanisms,[41] a deeper study of the upstream regulation of Akt in the IUE-induced neoplasms represents an intriguing task for future research.

BRAF^{V600E}/*p*Akt tumors require only a single additional genetic hit given by *Trp53*-loss to acquire anaplasia. The malignancy of these tumors is also documented by their rapid growth and short survival of mice compared to other high-grade neuroepithelial tumor variants in mouse models including invasive high-grade gliomas, medulloblastoma, or adult glioma.[42,43] Since *BRAF*^{V600E}/*p*Akt/*Tp53*^{KO} neoplasms still encounter pronounced dysmorphic neurons, these tumors recapitulate clear anaplastic GG features, rather than characteristics of (epitheloid) glioblastoma or anaplastic xanthoastrocytoma. Genetic multicolor labeling of tumor cells indicates that the *BRAF*^{V600E}/*p*Akt/*Tp53*^{KO} neoplasms are multiclonal and derive from pluripotent neural precursors capable of giving rise to dysplastic neurons and neoplastic astroglia.

The transcriptional profile of the *BRAF*^{V600E}/*p*Akt/*Trp53*^{KO} tumors strongly reflects their malignant biological behavior and invasive growth. Furthermore, pronounced transcript signatures relate to immune processes. Thus, augmented transcript patterns in *BRAF*^{V600E}/*p*Akt/*Trp53*^{KO} tumors share major GO-term signatures with human malignant gliomas of mesenchymal subtype,[31] which frequently harbor mutations of *Trp53* and *NF1*, the latter resulting in aberrant Ras/MAPK- and mTOR-pathway activation.[44] In addition, there is reduced expression of transcripts related to synaptic structural homeostasis and transmission, of potassium and calcium channels, neurotransmitter receptors, and GABAergic inhibition despite the presence of a substantial dysmorphic neuronal component in *BRAF*^{V600E}/*p*Akt/*Trp53*^{KO} neoplasms. Compromised inhibition related to reduced expression of GABA homeostasis-relevant molecules including GABA receptor and chloride potassium transporter transcripts has also been previously demonstrated in the microenvironment of gliomas.[32] Thus, dysregulation of inhibitory circuits represents a common phenomenon in different brain tumors.[7]

With respect to electrical activity, the present data suggest as unique for the *BRAF*^{V600E}/*p*Akt tumors spike frequencies in the core region resembling activity in pre-existing cortex. This might be unexpected as the cellular architecture is characterized by dysmorphic neurons and neoplastic astrocytes and thus differs from the normal cortex. Intriguingly, *BRAF*^{V600E} expressed under GLAST/Nestin promoters was demonstrated to confer a hyperexcitable phenotype to pyramidal neurons.[30] We propose that this cellular hyperexcitability of *BRAF*^{V600E}-positive neurons functionally compensates for the distorted network architecture to yield almost normal spike rates in the tumor core region. Spikes generated in this core tumor area will have a high propensity to propagate to neighboring cortical areas because the peri-tumoral region of *BRAF*^{V600E}/*p*Akt tumors amplifies activity (Figure 6G). As a consequence, the combination of maintained central neuronal activity with an enhanced relay to adjacent normal tissue will render this model most susceptible for the emergence of epileptiform activity.

Our results show that both 1- and 3-hit neoplasms lack significant intrinsic spike activity, which appears in line with the predominant glial differentiation of the former and a chaotic, dysfunctional cellular composition combined with reduced expression of transcripts instrumental for neuronal signaling in the latter. This observation is not contradictory to the fact that human PLNTYs are frequently associated with epilepsy.[5] It is noteworthy in this context that Pallud et al demonstrated recordings with epileptiform activity largely absent in human epileptogenic low-grade gliomas

Fig. 6, continued
visualization defined by category of the number of spikes per electrode for *BRAF*^{V600E}, *BRAF*^{V600E}/*p*Akt, *BRAF*^{V600E}/*p*Akt/*Trp53*^{KO}, and control slices incubated with aCSF. Time bin = 10 s. Connecting lines are color-coded according to the category they belong to. (E) Representative traces of spontaneous firing from slices incubated with aCSF for 80 µs. (F) Inter-model comparison of the mean of number of spikes per electrode from acute slices incubated with aCSF (N = 3-6; n = 7-21). (G) Inter-model comparison of the mean number of spikes per electrode of brain slices incubated with aCSF (low Mg^{2+}, high K$^+$). One-way ANOVA followed by Tukey's multiple comparison test). Abbreviations: aCSF, artificial cerebrospinal fluid; GG, ganglioglioma; MEA, multielectrode array.

but strongly present in surrounding brain tissue.[32] Such pathogenetic conditions may account for PLNTYs as well.

Future studies will have to decipher the roles of secreted factors and synaptic inputs from the tumor environment present in diffuse gliomas[33,34] for the *BRAF^V600E*-induced tumor spectrum. Our present data explain the molecular basis underlying heterogeneity of *BRAF^V600E*-positive brain tumors and provides vistas for tailored therapy development.

Supplementary Material

Supplementary material is available at *Neuro-Oncology* online.

Keywords

dysplastic neuron | epileptogenicity | neoplastic astroglia | pediatric tumor

References

1. Chappé C, Padovani L, Scavarda D, et al. Dysembryoplastic neuroepithelial tumors share with pleomorphic xanthoastrocytomas and ganglioliomas *BRAF^V600E* mutation and expression. *Brain Pathol.* 2013;23(5):574–583.

2. Dougherty MJ, Santi M, Brose MS, et al. Activating mutations in BRAF characterize a spectrum of pediatric low-grade gliomas. *Neuro Oncol.* 2010;12(7):621–630.

3. Schindler G, Capper D, Meyer J, et al. Analysis of *BRAF* V600E mutation in 1,320 nervous system tumors reveals high mutation frequencies in pleomorphic xanthoastrocytoma, ganglioglioma and extra-cerebellar pilocytic astrocytoma. *Acta Neuropathol.* 2011;121(3):397–405.

4. Qaddoumi I, Orisme W, Wen J, et al. Genetic alterations in uncommon low-grade neuroepithelial tumors: *BRAF*, *FGFR1*, and *MYB* mutations occur at high frequency and align with morphology. *Acta Neuropathol.* 2016;131(6):833–845.

5. Huse JT, Snuderl M, Jones DT, et al. Polymorphous low-grade neuroepithelial tumor of the young (PLNTY): an epileptogenic neoplasm with oligodendroglioma-like components, aberrant CD34 expression, and genetic alterations involving the MAP kinase pathway. *Acta Neuropathol.* 2017;133(3):417–429.

6. Koelsche C, Wöhrer A, Jeibmann A, et al. Mutant BRAF V600E protein in ganglioglioma is predominantly expressed by neuronal tumor cells. *Acta Neuropathol.* 2013;125(6):891–900.

7. Blumcke I, Spreafico R, Haaker G, et al.; EEBB Consortium. Histopathological findings in brain tissue obtained during epilepsy surgery. *N Engl J Med.* 2017;377(17):1648–1656.

8. Blümcke I, Aronica E, Becker A, et al. Low-grade epilepsy-associated neuroepithelial tumours—the 2016 WHO classification. *Nat Rev Neurol.* 2016;12(12):732–740.

9. Koh HY, Kim SH, Jang J, et al. *BRAF* somatic mutation contributes to intrinsic epileptogenicity in pediatric brain tumors. *Nat Med.* 2018;24(11):1662–1668.

10. Boer K, Troost D, Timmermans W, van Rijen PC, Spliet WG, Aronica E. Pi3K-mTOR signaling and AMOG expression in epilepsy-associated glioneuronal tumors. *Brain Pathol.* 2010;20(1):234–244.

11. Majores M, Schick V, Engels G, et al. Mutational and immunohistochemical analysis of ezrin-, radixin-, moesin- (ERM) molecules in epilepsy-associated glioneuronal lesions. *Acta Neuropathol.* 2005;110(6):537–546.

12. Rak B, Szlufik S, Grajkowska W, et al. Upregulation of mitogen-activated protein kinase in ganglioglioma. *Folia Neuropathol.* 2013;51(4):283–289.

13. Prabowo AS, Iyer AM, Veersema TJ, et al. BRAF V600E mutation is associated with mTOR signaling activation in glioneuronal tumors. *Brain Pathol.* 2014;24(1):52–66.

14. Hirose T, Scheithauer BW, Lopes MB, Gerber HA, Altermatt HJ, VandenBerg SR. Ganglioglioma: an ultrastructural and immunohistochemical study. *Cancer.* 1997;79(5):989–1003.

15. Pandita A, Balasubramaniam A, Perrin R, Shannon P, Guha A. Malignant and benign ganglioglioma: a pathological and molecular study. *Neuro Oncol.* 2007;9(2):124–134.

16. Fukushima T, Katayama Y, Watanabe T, Yoshino A, Komine C, Yokoyama T. Aberrant TP53 protein accumulation in the neuronal component of ganglioglioma. *J Neurooncol.* 2005;72(2):103–106.

17. Zanello M, Pagès M, Roux A, et al. Epileptic seizures in anaplastic gangliogliomas. *Br J Neurosurg.* 2017;31(2):227–233.

18. Rossini L, Villani F, Granata T, et al. FCD type II and mTOR pathway: evidence for different mechanisms involved in the pathogenesis of dysmorphic neurons. *Epilepsy Res.* 2017;129:146–156.

19. Kaul A, Chen YH, Emnett RJ, Dahiya S, Gutmann DH. Pediatric glioma-associated *KIAA1549:BRAF* expression regulates neuroglial cell growth in a cell type-specific and mTOR-dependent manner. *Genes Dev.* 2012;26(23):2561–2566.

20. Roux PP, Shahbazian D, Vu H, et al. RAS/ERK signaling promotes site-specific ribosomal protein S6 phosphorylation via

RSK and stimulates cap-dependent translation. *J Biol Chem.* 2007;282(19):14056–14064.

21. Aoki M, Batista O, Bellacosa A, Tsichlis P, Vogt PK. The Akt kinase: molecular determinants of oncogenicity. *Proc Natl Acad Sci U S A.* 1998;95(25):14950–14955.

22. Chen F, Becker A, LoTurco J. Sources of CNS tumor heterogeneity. *Oncoscience.* 2014;1(7):482–483.

23. Louis DN, Perry A, Reifenberger G, et al. The 2016 World Health Organization classification of tumors of the central nervous system: a summary. *Acta Neuropathol.* 2016;131(6):803–820.

24. Lang FF, Epstein FJ, Ransohoff J, et al. Central nervous system gangliogliomas. Part 2: clinical outcome. *J Neurosurg.* 1993;79(6):867–873.

25. Luyken C, Blümcke I, Fimmers R, Urbach H, Wiestler OD, Schramm J. Supratentorial gangliogliomas: histopathologic grading and tumor recurrence in 184 patients with a median follow-up of 8 years. *Cancer.* 2004;101(1):146–155.

26. Hayashi Y, Iwato M, Hasegawa M, Tachibana O, von Deimling A, Yamashita J. Malignant transformation of a gangliocytoma/ganglioglioma into a glioblastoma multiforme: a molecular genetic analysis. Case report. *J Neurosurg.* 2001;95(1):138–142.

27. Cai D, Cohen KB, Luo T, Lichtman JW, Sanes JR. Improved tools for the Brainbow toolbox. *Nat Methods.* 2013;10(6):540–547.

28. Livet J, Weissman TA, Kang H, et al. Transgenic strategies for combinatorial expression of fluorescent proteins in the nervous system. *Nature.* 2007;450(7166):56–62.

29. Raabe EH, Lim KS, Kim JM, et al. BRAF activation induces transformation and then senescence in human neural stem cells: a pilocytic astrocytoma model. *Clin Cancer Res.* 2011;17(11):3590–3599.

30. Goz RU, Silas A, Buzel S, LoTurco JJ. *BRAF*^{V600E} expression in mouse neuroglial progenitors increase neuronal excitability, cause appearance of balloon-like cells, neuronal mislocalization, and inflammatory immune response. *bioRxiv*, doi:10.1101/544973, February 15, 2019, preprint: not peer reviewed.

31. Verhaak RG, Hoadley KA, Purdom E, et al.; Cancer Genome Atlas Research Network. Integrated genomic analysis identifies clinically relevant subtypes of glioblastoma characterized by abnormalities in *PDGFRA*, *IDH1*, *EGFR*, and *NF1*. *Cancer Cell.* 2010;17(1):98–110.

32. Pallud J, Le Van Quyen M, Bielle F, et al. Cortical GABAergic excitation contributes to epileptic activities around human glioma. *Sci Transl Med.* 2014;6(244):244ra89.

33. Venkatesh HS, Morishita W, Geraghty AC, et al. Electrical and synaptic integration of glioma into neural circuits. *Nature.* 2019;573(7775):539–545.

34. Venkataramani V, Tanev DI, Strahle C, et al. Glutamatergic synaptic input to glioma cells drives brain tumour progression. *Nature.* 2019;573(7775):532–538.

35. Kalyan-Raman UP, Olivero WC. Ganglioglioma: a correlative clinicopathological and radiological study of ten surgically treated cases with follow-up. *Neurosurgery.* 1987;20(3):428–433.

36. Surrey LF, Jain P, Zhang B, et al. Genomic analysis of dysembryoplastic neuroepithelial tumor spectrum reveals a diversity of molecular alterations dysregulating the MAPK and PI3K/mTOR pathways. *J Neuropathol Exp Neurol.* 2019;78(12):1100–1111.

37. Gronych J, Korshunov A, Bageritz J, et al. An activated mutant BRAF kinase domain is sufficient to induce pilocytic astrocytoma in mice. *J Clin Invest.* 2011;121(4):1344–1348.

38. Siddiqi F, Chen F, Aron AW, Fiondella CG, Patel K, LoTurco JJ. Fate mapping by piggyBac transposase reveals that neocortical GLAST+ progenitors generate more astrocytes than Nestin+ progenitors in rat neocortex. *Cereb Cortex.* 2014;24(2):508–520.

39. Sokolov AM, Seluzicki CM, Morton MC, Feliciano DM. Dendrite growth and the effect of ectopic Rheb expression on cortical neurons. *Neurosci Lett.* 2018;671:140–147.

40. Iffland PH 2nd, Baybis M, Barnes AE, Leventer RJ, Lockhart PJ, Crino PB. DEPDC5 and NPRL3 modulate cell size, filopodial outgrowth, and localization of mTOR in neural progenitor cells and neurons. *Neurobiol Dis.* 2018;114:184–193.

41. Banerjee S, Byrd JN, Gianino SM, et al. The neurofibromatosis type 1 tumor suppressor controls cell growth by regulating signal transducer and activator of transcription-3 activity in vitro and in vivo. *Cancer Res.* 2010;70(4):1356–1366.

42. Pathania M, De Jay N, Maestro N, et al. H3.3^{K27M} cooperates with *Trp53* loss and PDGFRA gain in mouse embryonic neural progenitor cells to induce invasive high-grade gliomas. *Cancer Cell.* 2017;32(5):684–700.e9.

43. Alcantara Llaguno S, Chen J, Kwon CH, et al. Malignant astrocytomas originate from neural stem/progenitor cells in a somatic tumor suppressor mouse model. *Cancer Cell.* 2009;15(1):45–56.

44. Johannessen CM, Reczek EE, James MF, Brems H, Legius E, Cichowski K. The NF1 tumor suppressor critically regulates TSC2 and mTOR. *Proc Natl Acad Sci U S A.* 2005;102(24):8573–8578.